

Research Article

Int J Energy Studies, 2022; 7(1): 21-48

Received: 20 Jan 2022

Revised: 21 Feb 2022

Accepted: 03 Mar 2022

Computational study of combustion characteristics and flame stability of a cavity-stabilized burner

Junjie Chen *

Department of Energy and Power Engineering, School of Mechanical and Power Engineering, Henan Polytechnic University, 2000 Century Avenue, Jiaozuo, Henan, 454000, P.R. China, ORCID Number: 0000-0002-4222-1798
(*Corresponding Author: cjjtpj@163.com)

Highlights

- Combustion is stabilized by recirculation of hot combustion products induced by the cavity structure.
- The inlet velocity is a critical factor in assuring flame stability.
- The thermal conductivity of the burner walls plays a vital role in flame stability.
- Burners with large dimensions lead to a delay in flame ignition and may cause blowout.
- There are issues of efficiency loss for fuel-rich combustion cases.

You can cite this article as: Chen, J. “Computational study of combustion characteristics and flame stability of a cavity-stabilized burner”, *International Journal of Energy Studies* 2022; 7(1); 21-48.

ABSTRACT

A fundamental understanding of the stabilization mechanisms of a flame within very small spaces by the cavity method is of both fundamental and practical significance. However, the precise mechanism by which the cavity method generally provides increased flame stability remains unclear and warrants further study. This study relates to the combustion characteristics and flame stability of a micro-structured cavity-stabilized burner. Numerical simulations are conducted to gain insights into burner performance such as temperatures, reaction rates, species concentrations, and flames. The effects of different design parameters on flame stability are investigated. The criteria factors affecting combustion characteristics and flame stability are determined. Design recommendations are provided. The results indicate that the inlet velocity of the mixture is a critical factor in assuring flame stability within the cavity-stabilized burner. There is a narrow range of inlet velocities that permit sustained combustion within the cavity-stabilized burner. Fast flows can cause blowout and slow flows can cause extinction. There exists an optimum inlet velocity for greatest flame stability. The combustion is stabilized by recirculation of hot combustion products induced by the cavity structure. The thermal conductivity of the burner walls plays a vital role in flame stability. Improvements in flame stability are achievable by using walls with anisotropic thermal conductivity. Burner dimensions greatly affect flame stability. Burners with large dimensions lead to a delay in flame ignition and may cause blowout. Heat-insulating materials are favored to minimize external heat losses. There are issues of efficiency loss for fuel-rich combustion cases.

Keywords: Stabilization mechanisms, Thermal conductivity, Critical factors, Blowout, Extinction

1. INTRODUCTION

Compact, highly mobile, and efficient thermodynamic and energy systems are becoming increasingly important for a wide range of applications [1, 2], such as thermodynamic cycling of distributed ventilation and heating systems, modular propulsion and control of self-powered and distributed sensor and actuation systems [3, 4], and cooling and powering of portable medical, communications, and electronics devices [5, 6], and many other applications. Generally, such applications optimally require power sources that are cost effective, and that are characterized by high energy density and power [7, 8] but minimal weight and dimensions.

Micro-structured combustion systems may overcome limitations of traditional thermodynamic and power sources [9, 10] by providing micromachinery components that enable efficient operation of thermodynamic systems and production of significant power in the regime of millimeters [11, 12] to meet the cost, weight, modularity, mobility, and efficiency requirements of a wide range of modern applications. For example, micro-structured combustion systems can provide power sources that can be employed in a wide range of portable electric power applications [13, 14] such as portable coolers, heaters, communication and electronic devices, and other such applications. More particularly, micro-structured combustion systems enable realization of a wide range of micromachinery componentry for thermodynamic cycling, propulsion, and producing sources of power that achieve high efficiencies of components [15, 16]. Micro-heat exchangers [17, 18], micro-turbines, micro-combustors [19, 20], and other micro-componentry can be developed as thermodynamic micro-modules that could be interconnected in various combinations to construct micro-structured thermodynamic cycles such as micro-gas turbine generators [21, 22], micro-gas turbine engines [23, 24], and a wide range of other thermodynamic cycles [25, 26] in the regime of millimeters. Specifically, micro-structured combustion systems are applicable to all portable electric power applications for which air is available [27, 28]. The very low noise produced by micro-structured combustion systems makes them particularly attractive from a practical perspective for applications such as military reconnaissance and office electronics [29, 30]. Micro-structured combustion systems can be further advantageously employed in manned mobile scenarios [31, 32]. Micro-structured combustion systems can similarly be employed to power implanted medical devices, for example, pace makers.

Unfortunately, flame stabilization is a common problem in micro-structured combustion systems [33, 34]. To achieve improvements in flame stability, various methods have been tried either

commercially or experimentally [35, 36] and many different structures have already been designed for micro-structured combustion systems [37, 38]. The typical method includes the use of recirculation regions to provide a continuous ignition source by mixing the hot combustion products with the cold incoming fuel and air mixture. Structural devices have been commonly employed to establish a recirculation region for improving the stability of the flame during ignition and operation, for example, cavities [39, 40]. A fundamental understanding of the stabilization mechanisms of a flame within very small spaces by the cavity method is of both fundamental and practical significance. However, the precise mechanism by which the cavity method generally provides increased flame stability remains unclear and warrants further study.

This study relates to the combustion characteristics of a micro-structured cavity-stabilized burner. Numerical simulations are conducted to gain insights into burner performance such as temperatures, reaction rates, species concentrations, and flames. The effects of inlet velocity, equivalence ratio, wall thermal conductivity, channel height, and heat transfer coefficient on flame stability are investigated. The factors affecting combustion characteristics are determined for the cavity-stabilized burner. Particular focus is placed on determining essential factors that affect the performance of the burner.

2. COMPUTATIONAL METHODS

2.1. Physical model

The use of a cavity configuration is particularly advantageous when arranged as a disturbance factor for a millimeter-scale burner. The millimeter-scale burner designed with cavities is depicted schematically in Figure 1. A lean methane-air mixture is conducted through a combustion chamber defined by parallel plates. The length of the channel is 50 mm, the height is 3 mm, and the width is 13 mm. A sudden cross section change of the axial flow cross section is present along the length of the cavity-stabilized burner. The depth of the cavities is 1.5 mm, the width of the cavities is 4 mm, and the distance away from the entrance is 10 mm. The angle of the cavity is 45° , and the thickness of the plates is 3 mm, as depicted schematically in Figure 1. The initial temperature is 1500 K, with a Reynolds number greater than 500 at the inlet. Due to the small internal space of the cavity-stabilized burner, the gas flow rate is small. Therefore, gas radiation and volume force are ignored in the model.

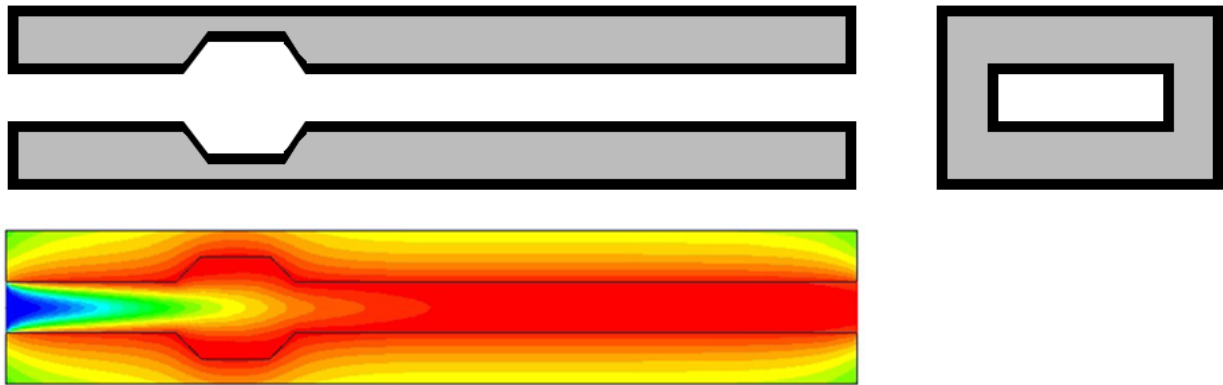


Figure 1. Schematic illustration of the millimeter-scale combustion system designed with cavities on the channel walls.

2.2. Mathematical model

The length scale of the burner is 3 mm for the combustion problem. In all the cases studied, the Reynolds number is less than 1270 due to the very small scale of the system, causing the gases to flow into the chamber in a laminar flow regime. The mathematical model is solved and implemented in ANSYS FLUENT to obtain the problem solution. ANSYS FLUENT permits multi-dimensional modeling of physical and chemical phenomena in the processes [41, 42], and various modes of heat transfer can be modeled. ANSYS FLUENT provides comprehensive modeling capabilities for a wide range of laminar flow problems. In ANSYS FLUENT, a broad range of mathematical models for transport phenomena is combined with the ability to model the geometry, including heat transfer and chemical reactions.

Continuity equation:

$$\frac{\partial}{\partial x}(\rho v_x) + \frac{\partial}{\partial y}(\rho v_y) = 0 \quad (1)$$

where v is the velocity, ρ is the density, and x and y denote Cartesian coordinates.

Momentum conservation equations:

$$\frac{\partial(\rho v_x v_x)}{\partial x} + \frac{\partial(\rho v_x v_y)}{\partial y} = -\frac{\partial p}{\partial x} + \frac{\partial \tau_{xx}}{\partial x} + \frac{\partial \tau_{xy}}{\partial y} \quad (2)$$

$$\frac{\partial(\rho v_y v_x)}{\partial x} + \frac{\partial(\rho v_y v_y)}{\partial y} = -\frac{\partial p}{\partial y} + \frac{\partial \tau_{yx}}{\partial x} + \frac{\partial \tau_{yy}}{\partial y} \quad (3)$$

where τ is the stress tensor.

Energy conservation equation:

$$\frac{\partial(\rho v_x h)}{\partial x} + \frac{\partial(\rho v_y h)}{\partial y} = \frac{\partial(k_f \partial T)}{\partial x^2} + \frac{\partial(k_f \partial T)}{\partial y^2} + \sum_i \left[\frac{\partial}{\partial x} \left(h_i \rho D_i \frac{\partial Y_i}{\partial x} \right) + \frac{\partial}{\partial y} \left(h_i \rho D_i \frac{\partial Y_i}{\partial y} \right) \right] + \sum_i h_i R_i \quad (4)$$

where h is the enthalpy, k is the thermal conductivity, T is the temperature, Y is the mass fraction, D is the molecular diffusivity, R is the reaction rate, and f denotes the fluid.

Species conservation equation:

$$\frac{\partial(\rho Y_i v_x)}{\partial x} + \frac{\partial(\rho Y_i v_y)}{\partial y} = \frac{\partial}{\partial x} \left(\rho D_{i,m} \frac{\partial Y_i}{\partial x} \right) + \frac{\partial}{\partial y} \left(\rho D_{i,m} \frac{\partial Y_i}{\partial y} \right) + R_i \quad (5)$$

ANSYS FLUENT predicts the local mass fraction of each species.

Solid energy conservation equation:

$$\frac{\partial}{\partial x} \left(k_s \frac{\partial T}{\partial x} \right) + \frac{\partial}{\partial y} \left(k_s \frac{\partial T}{\partial y} \right) = 0 \quad (6)$$

where s denotes the solid walls.

2.3. Chemical kinetic model

Theoretical information about finite-rate chemistry as related to the volumetric combustion reaction is presented here. The laminar finite-rate model computes the chemical source terms using Arrhenius expressions, and ignores the effects of turbulent fluctuations. The model is exact for laminar flames, but is generally inaccurate for turbulent flames due to highly non-linear Arrhenius chemical kinetics. In the present study, the gases flow through the channel in a laminar flow regime, as noted above. Therefore, the laminar finite-rate model is used to compute the chemical source terms. The reaction rate expression can be written as follows [43]:

$$r_{\text{CH}_4} \left[\text{kmol} \cdot \text{m}^{-3} \cdot \text{s}^{-1} \right] = 2.119 \times 10^{11} \cdot \exp \left[-\frac{2.027 \times 10^8}{RT} \right] \cdot [\text{CH}_4]^{0.2} \cdot [\text{O}_2]^{1.3} \quad (7)$$

where the unit of reaction rate is the $\text{kmol}/(\text{m}^3 \cdot \text{s})$, the unit of activation energy is J/kmol , and the unit of concentration is kmol/m^3 . This chemical kinetic model can be used to accurately describe flame dynamics and flame responses to external perturbations [44]. Thermal effects can be relatively well captured by the chemical kinetic model. ANSYS FLUENT can model the transport of chemical species by solving conservation equations describing convection, diffusion, and reaction sources for each component species.

2.4. Design parameters

The design parameters of the cavity-stabilized burner are summarized in Table 1. To avoid a negative effect on the combustion conditions, the design parameters must be selected with respect to each other in such a way that the highest stability is achieved for the methane flame. The influences are investigated by varying a particular design parameter while maintaining the other design parameters.

Table 1. Design parameters of the millimeter-scale cavity-stabilized combustion systems used in the computational fluid dynamics modeling

Variables	Inlet velocity (m/s)	Equivalence ratio	Thermal conductivity (W/(m·K))	Channel height (mm)	Heat transfer coefficient (W/(m ² ·K))
Effect of thermal conductivity	0.3	1.0	0.5, 1.4, 50, 50-0.5, 200	3	10
Effect of equivalence ratio	0.3	0.4, 0.6, 0.8, 1.0, 1.2	1.4	3	10
Effect of inlet velocity	0.1, 0.3, 0.5, 0.7	1.0	1.4	3	10
Effect of heat transfer coefficient	0.3	1.0	1.4	3	10, 20, 40, 60
Effect of channel height	0.3	1.0	1.4	3, 4, 5	10

Velocity inlet boundary conditions are used to define the velocity and scalar properties of the flow at inlet boundaries. Pressure outlet boundary conditions are used to define the static pressure at flow outlets. Wall boundary conditions are used to bound fluid and solid regions. Symmetry boundary conditions are used since the physical geometry has mirror symmetry.

2.5. Typical mesh

The typical mesh used for the cavity-stabilized burner is illustrated in Figure 2. More nodes are accumulated around the cavity structure and around the reaction regions. In total, the typical mesh consists of 36000 nodes for the cavity-stabilized burner. A mesh independence test is performed to assure independence of the solution. The fluid centerline temperature profiles are presented in

Figure 3 for meshes with different nodal densities. The inlet velocity of the gases is 0.6 m/s, with a stoichiometric fuel-air ratio. As the mesh density increases, there is a convergence of the solution. Solutions obtained with a mesh consisting of 36000 nodes are reasonably accurate. Larger mesh densities, up to 72000 nodes, offer no obvious advantage.

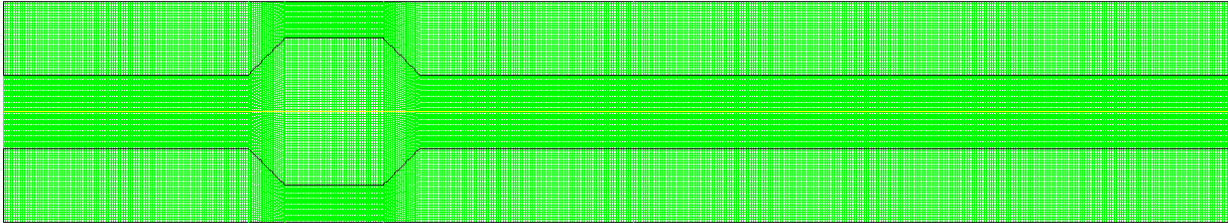


Figure 2. Typical mesh used for the cavity-stabilized burner. More nodes are placed around the cavity structure and around the reaction regions.

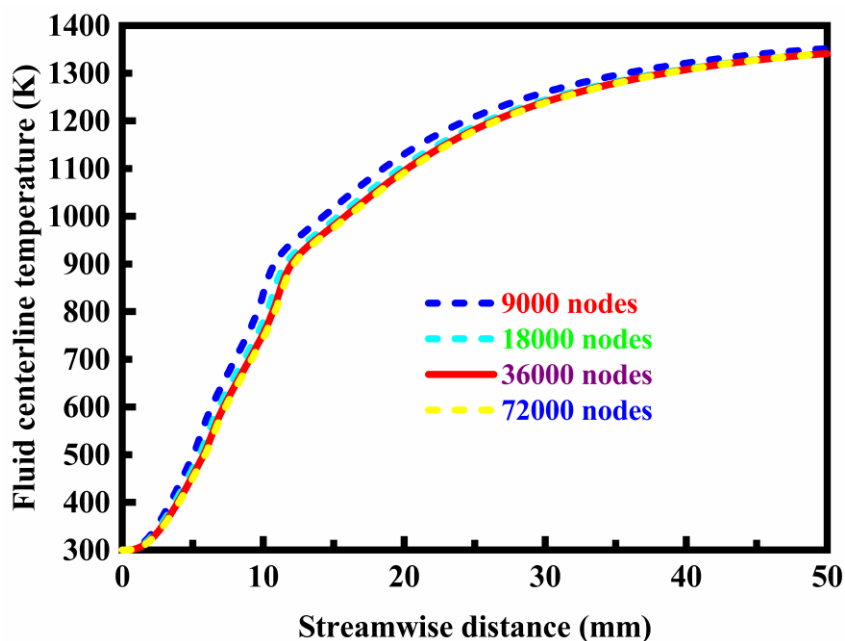


Figure 3. Fluid centerline temperature profiles for meshes with different nodal densities. The inlet velocity of the gases is 0.6 m/s, with a stoichiometric fuel-air ratio.

Successful computations of turbulent flows require some consideration during the mesh generation. Turbulent flow is often wall-bounded and the wall affects the flow significantly [45]. Consequently, the numerical results for turbulent flows tend to be more susceptible to mesh dependency than those for laminar flows. Accordingly, different strategies must be used in the vicinity of the wall depending on the chosen near-wall meshing [46]. In the present study, however, the gases flow through the cavity-stabilized channel in a laminar flow regime, as noted above. In

laminar flows, wall boundary conditions are used to bound fluid and solid regions and the no-slip boundary condition is enforced at walls.

2.6. Model validation

To verify the accuracy of the model, the predictions are compared with the data obtained from experimental measurements. The burner comprises two parallel fused-quartz plates. An ordinary camera is used to form an image using visible light, and a thermographic camera is used to create an image using infrared radiation. The thermographic camera can achieve a resolution of 640×480 pixels, and a temperature difference of 1.0 K at the scene induces a maximum temperature difference of 0.02 K at the sensor. The stable fluid centerline temperature profiles are determined from thermographic measurements using infrared radiation. A constant fuel-air stoichiometry is maintained in operation. The thermographic images acquired in the infrared spectral region, and the optical images in the visible spectral region, are presented in Figure 4. The contour plot of temperature in the burner is also presented in Figure 4. The fluid centerline temperature is plotted in Figure 5 against the streamwise distance. The fluid centerline temperature profiles are determined from thermographic measurements and predicted by the model. The predictions are in satisfactory agreement with the data obtained from experimental measurements.

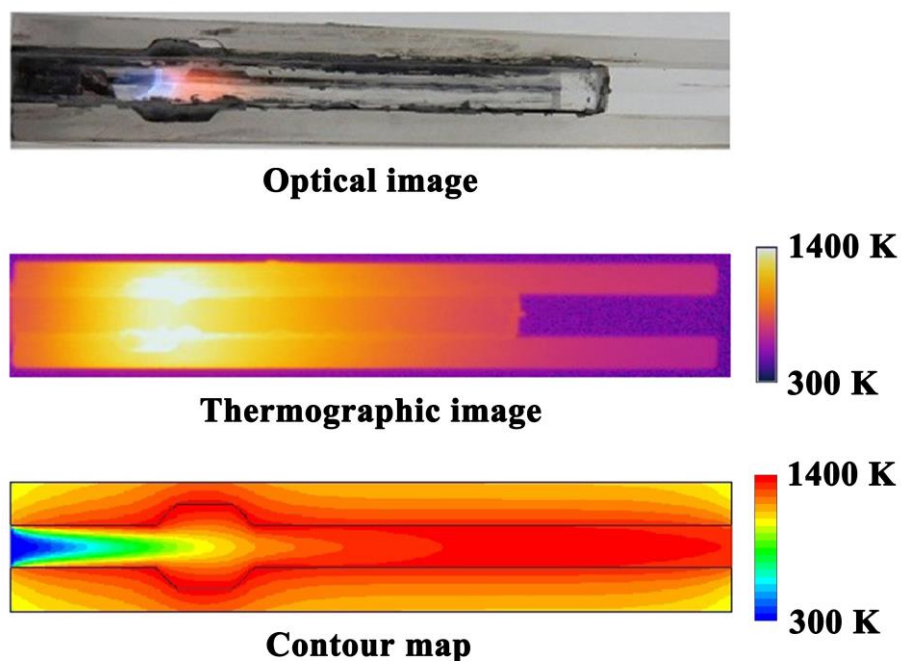


Figure 4. Laminar premixed methane flames and temperature variation in the burner. A constant fuel-air stoichiometry is maintained in operation.

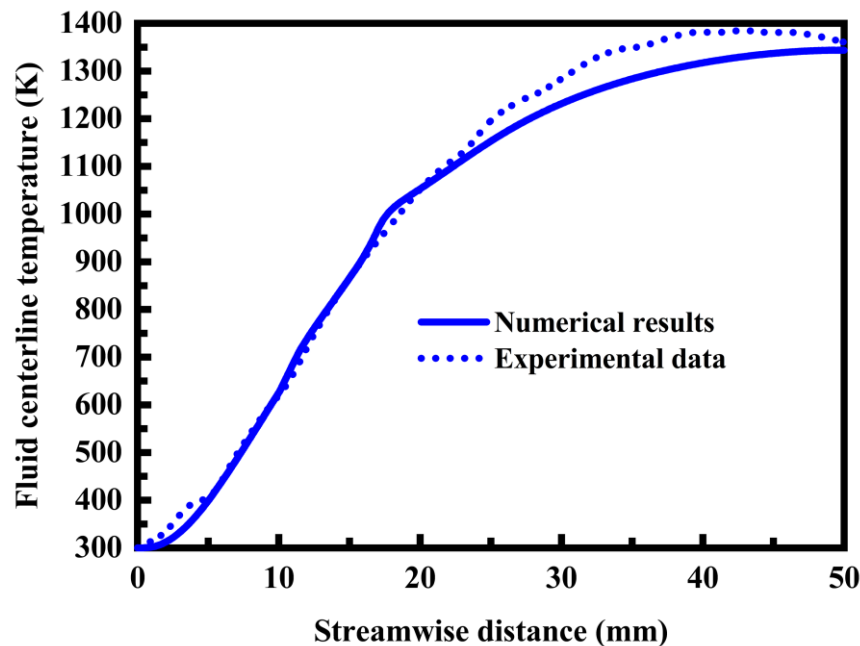


Figure 5. Fluid centerline temperature profiles determined from thermographic measurements and predicted by the model. A constant fuel-air stoichiometry is maintained in operation.

3. RESULTS AND DISCUSSION

3.1. Performance comparison

Prior to performing the computation, a comparison of methane conversion rate is carried out between a flat-plate burner and a cavity-stabilized burner. The composition change of the flat-plate burner and the cavity-stabilized burner is determined under the conditions of an equivalent ratio of 1.0, an inlet velocity of 0.5 m/s, and a wall thermal conductivity of 0.7 W/(m·K). The results are present in Figure 6, in which the axial fluid centerline temperature and the methane mass fraction are plotted against the streamwise distance. The fuel combusts in the burners in a predictable manner. For the cavity-stabilized burner, the fuel normally burns at relatively high temperatures, which inherently results in a improvement in flame stability. The methane conversion rate of the flat-plate burner is about 30%, and the methane conversion rate of the cavity-stabilized burner is about 90%. Therefore, the combustion efficiency of methane in the cavity-stabilized burner is higher than that of methane in the flat-plate burner. More complete combustion can be achieved in the cavity-stabilized burner. The flame stability of the flat-plate burner is trending towards becoming unstable. Even after ignition, it is difficult to maintain stable combustion in the flat-plate burner. Therefore, simply changing the combustor geometry to maintain near-stoichiometric ratios will avoid the loss of flame stability.

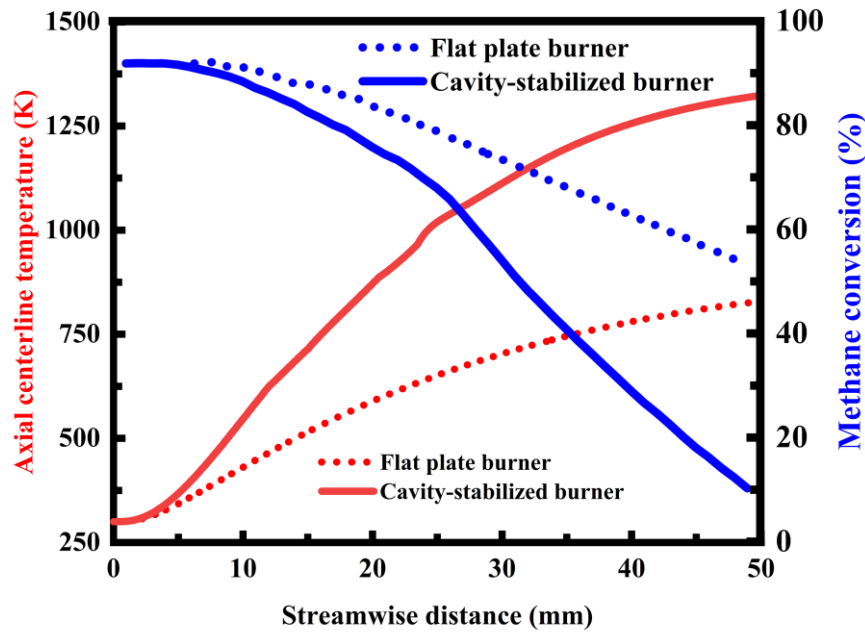


Figure 6. Axial fluid centerline temperature and methane mass fraction profiles along the length of the flat-plate and cavity-stabilized burners.

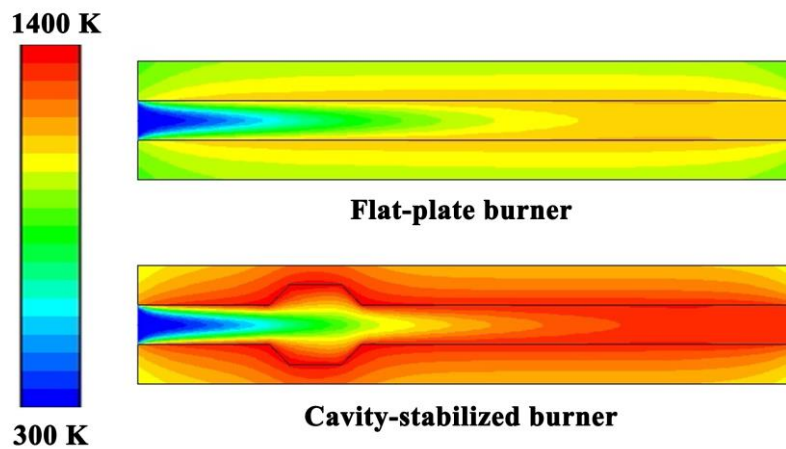


Figure 7. Contour plots of temperature for the flat-plate and cavity-stabilized burners. At room temperature, the thermal conductivity of the burner walls is 1.4 W/(m·K).

A recirculation region is established for the cavity-stabilized burner. As a result, the methane mass fraction is small at the outlet, and the axial fluid centerline temperature is higher than that in the flat-plate burner. Therefore, the cavity structure is usable for the stabilization of the methane flame, and the burner designed in such a way enable operation at a substantially higher temperature than the flat-plate burner. The contour plots of temperature are illustrated in Figure 7 for the flat-plate

and cavity-stabilized burners. An important feature of the cavity-stabilized burner is that high enough flame temperatures are achievable to permit effective use of the fuel, thereby raising the temperature to about 1400 K, which is much higher than that in the flat-plate burner. Under these circumstances, undesirable quantities of nitrogen oxides are nevertheless produced. Inasmuch as temperature and reaction rate are functionally related, an increase in temperature will lead to a corresponding increase in the reaction rate. As a result, rapid, efficient thermal combustion occurs in the cavity-stabilized burner. Such high reaction rates permit high fuel space velocities which normally are not obtainable in the flat-plate burner. Combustion of the admixture of gases is stabilized in the cavities. The combustion region is maintained downstream of the cavity structure, which is capable of creating a recirculation region to provide heat to the admixture of gases either through conduction or radiation. The cavity structure is usable for the stabilization of a flame, associated with an increase in temperature. Combustion is stabilized by recirculation of hot combustion products induced by the cavity structure. However, the cavity-stabilized burner has practical limits in terms of the cavity structure, since complexity is introduced into the design of the cavity-stabilized burner.

3.2. Effect of inlet velocity

The effect of changes in inlet velocity on burner temperature changes is investigated, and the axial fluid centerline temperature profiles are presented in Figure 8. Additionally, the effect of changes in velocity on methane conversion is illustrated in Figure 9. As the velocity increases, the residence time of the fuel in the burner becomes shorter. As the velocity increases, the convective timescale decreases, and a shift in the flame location downstream is observed, as expected. As the velocity increases, the position of the ignition point of the burner gradually moves away from the inlet to the outlet, as shown in Figure 8. This will lead to raise the temperature to about 1400 K, which may lead to the formation of substantial emissions of carbon monoxide and nitrogen oxides, particularly the latter. However, the formation of nitrogen oxides can be greatly reduced by limiting the residence time of the combustion products in the combustion region. At high inlet velocities, the system burns the fuel at relatively low temperatures. For fast velocities, the convective time scale becomes short compared to the axial conductive time scale. The wall takes a longer distance to preheat the mixture to the ignition temperature, which increases the flame location and may lead to blowout.

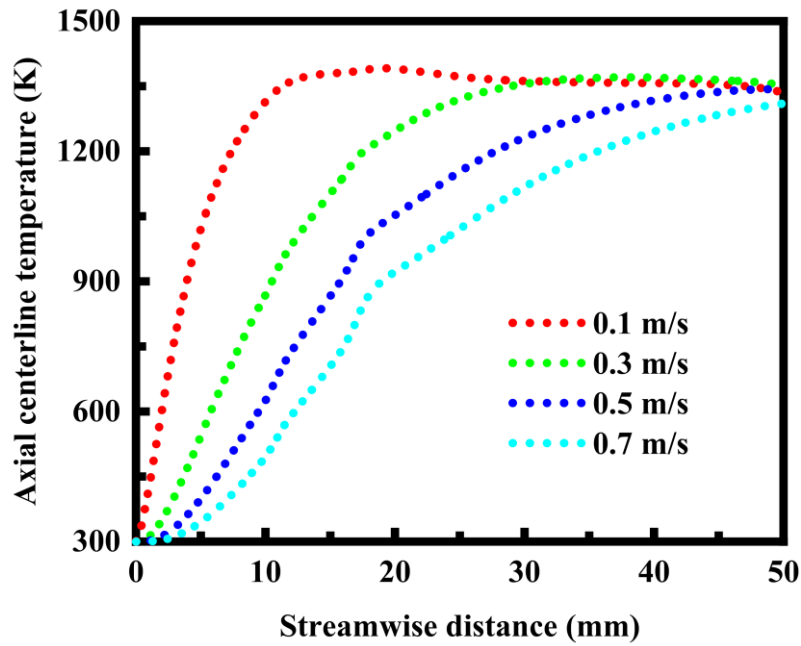


Figure 8. Axial fluid centerline temperature profiles along the length of the cavity-stabilized burner under different admixture inlet velocity conditions.

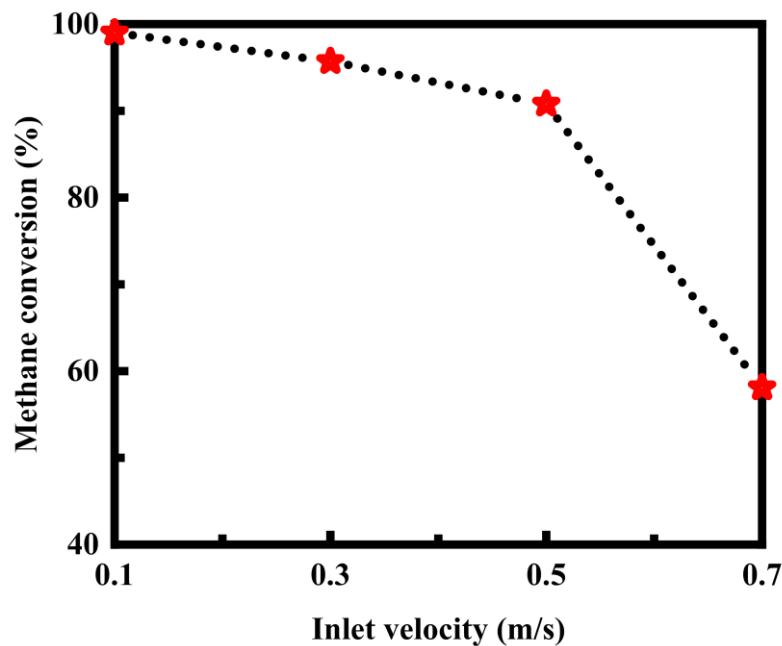


Figure 9. Effect of admixture inlet velocity on the methane conversion at the outlet of the cavity-stabilized burner.

The methane conversion rate increases with the velocity, as shown in Figure 9, thereby stabilizing combustion in the cavity-stabilized burner. Combustion is more readily stabilized in the cavity-stabilized burner at low velocities. Blowout will occur at sufficiently high velocities [47, 48].

Therefore, an appropriate velocity is very important for continuous stabilization of combustion in the cavity-stabilized burner. Cavity-stabilized combustion will tend to reduce unburned hydrocarbons emissions, as shown in Figure 9. Consequently, the velocity is a critical factor in assuring flame stability within the cavity-stabilized burner.

The axial centerline reaction rate profiles are presented in Figure 10 at different inlet velocities. As the velocity increases, the peak of the reaction rate along the fluid centerline gradually moves away from the inlet of the burner to the outlet. When the velocity is low, methane is substantially completely converted near the inlet of the burner, and the peak of the reaction rate is also close to the inlet. When the velocity is high, the flame shifts toward the outlet, and the fuel fails to fully react with air, as shown in Figure 10. In this case, the peak of the reaction rate is closer to the outlet. For fast flows, blowout occurs, whereas for slow flows, global type extinction occurs due to slow convective heat transfer. As a result, there exists an optimum inlet velocity for the highest reaction rate for which propagation of the flame is desired. The optimum inlet velocity is 0.3 m/s for the conditions studied here.

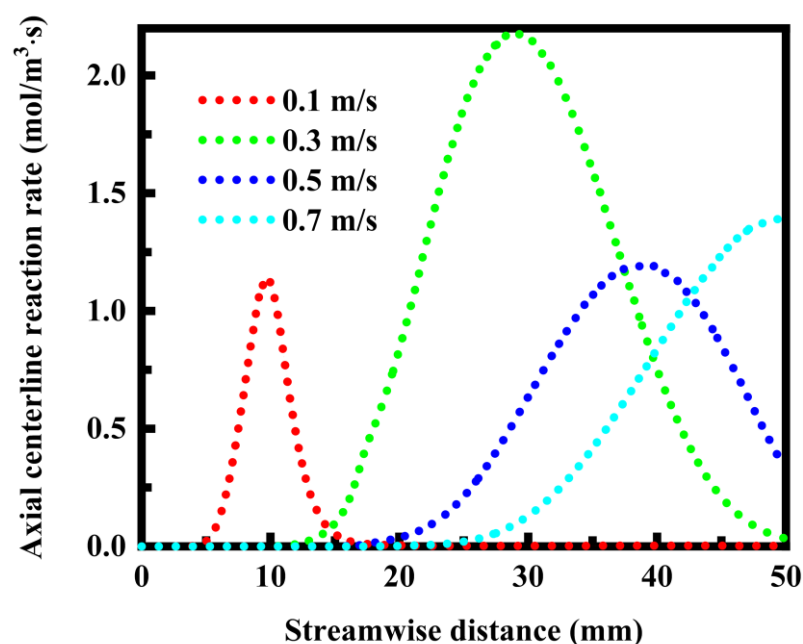


Figure 10. Axial centerline rate profiles of the combustion reaction in the cavity-stabilized burner under different admixture inlet velocity conditions.

The transverse rate profiles of the combustion reaction are presented in Figure 11 at different distances from the axial centerline. The velocity is 0.3 m/s. When the distance from the axial

centerline is 0.5 mm and 1.0 mm, the peak of the reaction rate generally occurs near the middle of the cavity-stabilized burner. When the position is near the inner wall surface, the peak of the reaction rate is close to the entrance of the cavity-stabilized burner. This is because when the velocity is low, the wall temperature is higher than the temperature of the central flow channel, and the gas near the wall can quickly absorb heat and reach the ignition temperature to react. The irregular change of the rate of the combustion reaction near the cavities is mainly due to the formation of low-speed recirculation regions, in which the heat and mass transfer in the cavities are uneven. Advantageously, the recirculation regions make the gas in the cavities flow violently, which facilitates the combustion process.

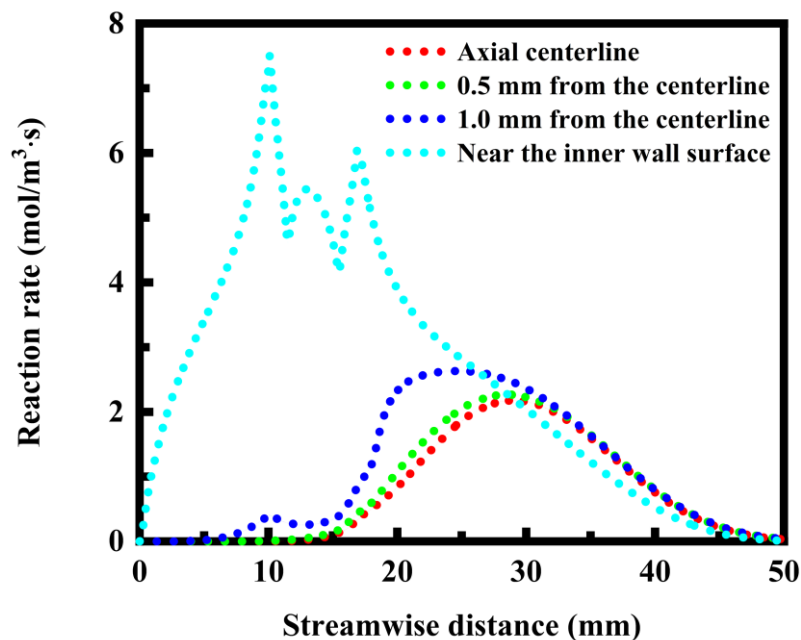


Figure 11. Transverse rate profiles of the combustion reaction at different distances from the axial centerline. The admixture inlet velocity is 0.3 m/s.

3.3. Effect of channel height

The major problem of the micro-structured burner is the high ratio of surface to volume [49, 50]. As the ratio of surface to volume increases, heat loss to the surroundings increases, which could eventually lead to flame quenching [51, 52]. Therefore, the effect of the dimensions of the burner, for example, channel height, is investigated to better understand the stability of flame in the cavity-stabilized burner. The change characteristics of the temperature along the outer wall surface of the burner and along the fluid centerline are presented in Figure 12 under different channel height conditions. As the height of the burner channel increases, the temperature of the axial centerline

of the burner decreases, and the ignition position of the flame is far away from the inlet position, which further reduces the efficiency of the combustion process. As the height of the burner channel increases, the temperature of the outer wall increases. This is because under the same conditions such as a flow velocity of 0.3 m/s and an equivalent ratio of 1.0, the amount of methane flowing into the channel per unit time increases with the channel height. As a result, the heat released by fuel combustion increases, and the temperature of the outer wall surface increases. However, the efficiency of the combustion process decreases with the channel height. As the height of the burner channel increases, the amount of unreacted fuel in the axial centerline becomes larger, and the incoming admixture of gases will absorb more heat for preheating. As a result, the temperature along the fluid centerline drops significantly. As the height of the burner channel decreases, designing the burner presents challenges resulting from greatly increased pressure drop across the channel and consequently a substantial loss of energy.

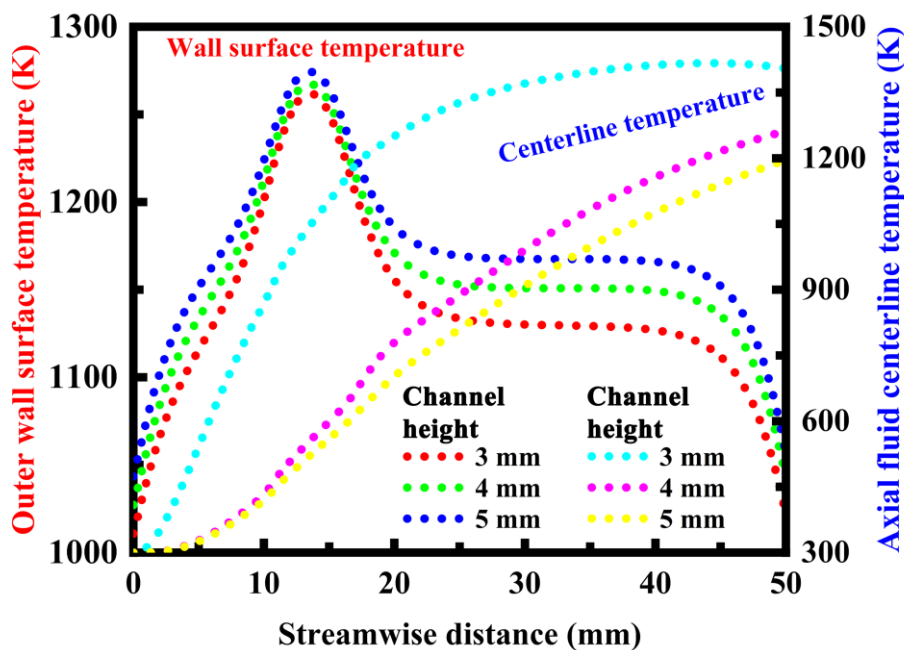


Figure 12. Temperature profiles along the outer wall surface of the cavity-stabilized burner and along the fluid centerline under different channel height conditions.

3.4. Effect of wall thermal conductivity

The contour plots of temperature are presented in Figure 13 at different thermal conductivities. The thermal conductivity of the solid material has little effect on the temperature of the fluid but has a strong effect on the temperature of the walls. The temperature gradient is steep within the walls with a low thermal conductivity. The temperature of the exterior walls typically increases

with the thermal conductivity. The solid material is advantageously thermally conductive to permit a high wall temperature with more uniform distribution. A portion of heat of reaction is transferred to the upstream structure of the burner by heat conduction through the walls, which is necessary for ignition and flame stability [47, 48]. The term anisotropy is used in Figure 13 to describe direction-dependent thermal conductivity of the solid material. In this case, the anisotropic solid material inhibits transverse but allows longitudinal heat conduction. The walls permit heat flux in the longitudinal direction to preheat the fluid, yet does not permit heat losses in the transverse direction to the surroundings.

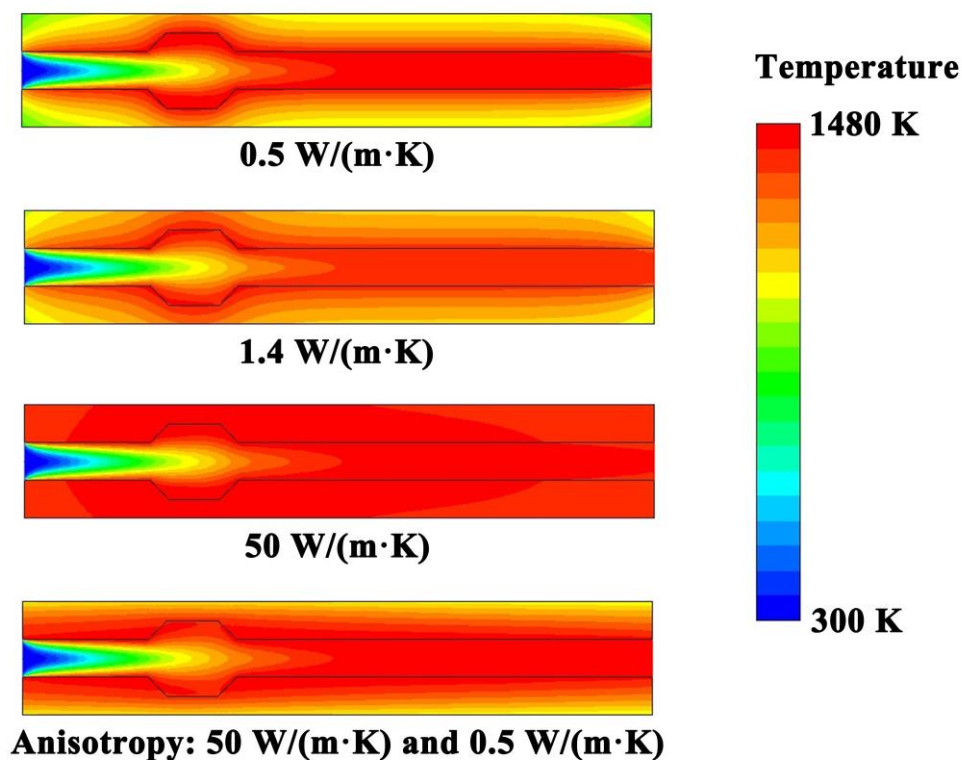


Figure 13. Contour plots of temperature at different thermal conductivities. The thermal conductivity of the anisotropic solid material is $50 \text{ W}/(\text{m}\cdot\text{K})$ in the longitudinal direction and $0.5 \text{ W}/(\text{m}\cdot\text{K})$ in the transverse direction.

The temperature change characteristics of the outer wall surface of the burner are illustrated in Figure 14 at different thermal conductivities. As the thermal conductivity increases, the temperature of the outer wall surface increases and the wall temperature distribution is more uniform. Ceramics with a high thermal conductivity may be employed for the burner. However, this increase in temperature results in a significant increase in heat losses. More specifically,

excessive temperature will cause a large amount of heat loss, which will cause unstable combustion performance. In addition, it is important to operate the burner at a safe temperature. When the thermal conductivity is low, the temperature of the outer wall surface is also low and the temperature distribution is uneven. This will be detrimental to the stability of the flame, and local thermal stress is prone to occur. To better solve the above problems, walls with anisotropic thermal conductivity can not only transfer heat upstream for preheating the low-temperature unreacted pre-mixed gas, but also reduce the large heat loss caused by excessive wall temperatures, which will lead to unstable combustion performance. Two-dimensional materials may have anisotropic thermal properties [53, 54], for example, graphene.

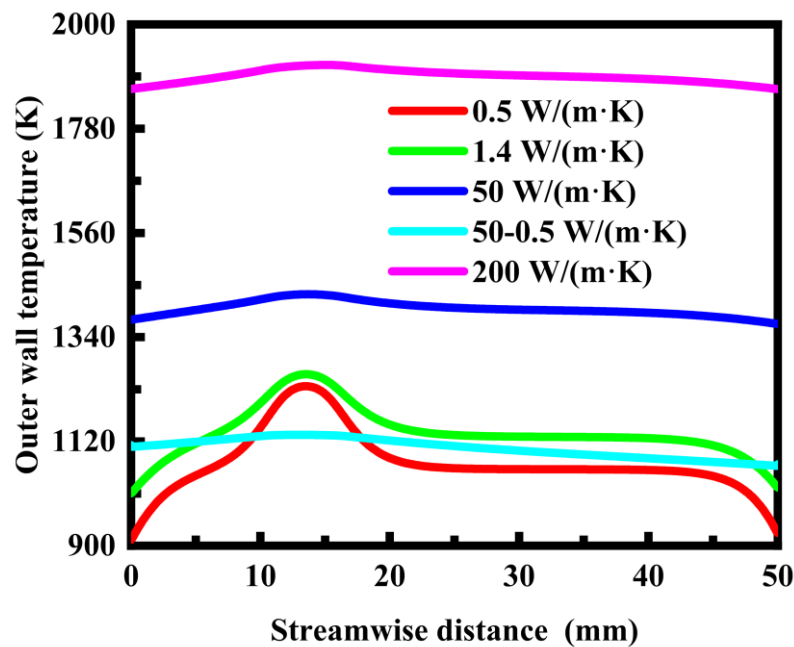


Figure 14. Temperature profiles along the outer wall surface of the cavity-stabilized burner under different thermal conductivity conditions.

The temperature profiles along the fluid centerline of the cavity-stabilized burner are presented in Figure 15 at different thermal conductivities. The thermal conductivity mainly affects the temperature of the burner wall surfaces as well as the rate of heat transfer, as discussed above. In contrast, the thermal conductivity has little effect on the temperature along the fluid centerline, as shown in Figure 15. However, walls with excessively large thermal conductivity may cause unstable combustion, large heat loss, and the methane flame moves toward the outlet. Additionally, the temperature along the fluid centerline is relatively low when the thermal conductivity is 200 W/(m·K), as shown in Figure 15, but the temperature at the outlet is relatively high. The difference

in temperature is small between the different thermal conductivity cases, except the highest thermal conductivity case. Further improvements are achievable by using walls with anisotropic thermal conductivity, as discussed above.

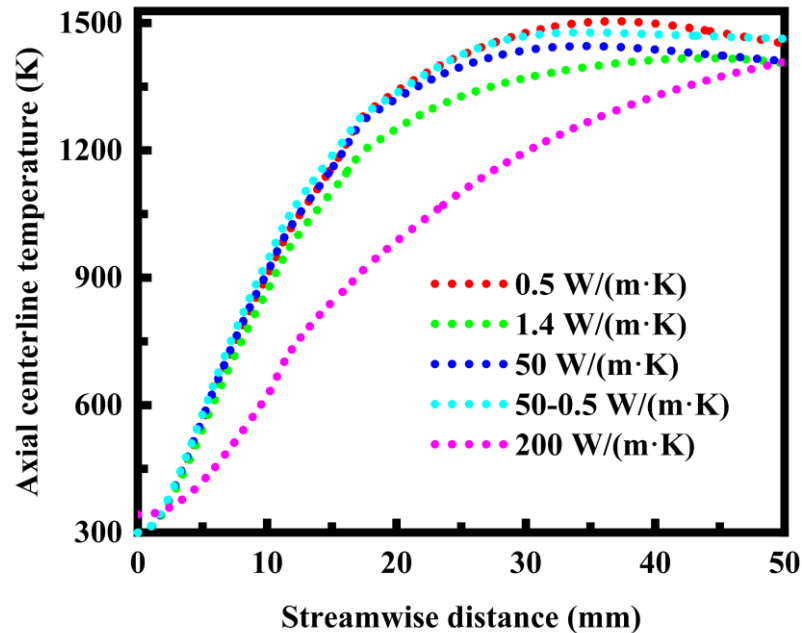


Figure 15. Temperature profiles along the fluid centerline of the cavity-stabilized burner under different thermal conductivity conditions.

3.5. Effect of wall heat transfer coefficient

The change characteristics of the temperature along the outer wall surface of the cavity-stabilized burner and along the fluid centerline are presented in Figure 16 under different wall heat transfer coefficient conditions. As the heat transfer coefficient between the solid surface and the environment is increased, the wall heat loss increases. As a result, both the temperature of the outer wall surface of the cavity-stabilized burner and the temperature along the fluid centerline decrease, which will lead to a drop in overall burner temperature, thereby reducing the combustion efficiency of the fuel. When the heat transfer coefficient between the solid surface and the environment is $10 \text{ W}/(\text{m}^2 \cdot \text{K})$, the highest temperatures are obtained at the outer wall surface and along the fluid centerline, which is essential for the function of the cavity-stabilized burner. With the increase of the heat transfer coefficient, the temperature of the outer wall surface decreases. At larger heat transfer coefficients, the drop in temperature become more pronounced. The difference in temperature between the axial fluid centerlines is much smaller than that in temperature between the outer wall surfaces. For example, near the cavities where the axial distance varies from 10 to

20 mm, the maximum difference is about 40 K between the axial fluid centerline temperatures, but the maximum difference is about 90 K between the outer wall surface temperatures. Therefore, the wall heat transfer coefficient has a small effect on the axial fluid centerline temperature, but it plays a consider role in the outer wall surface temperature.

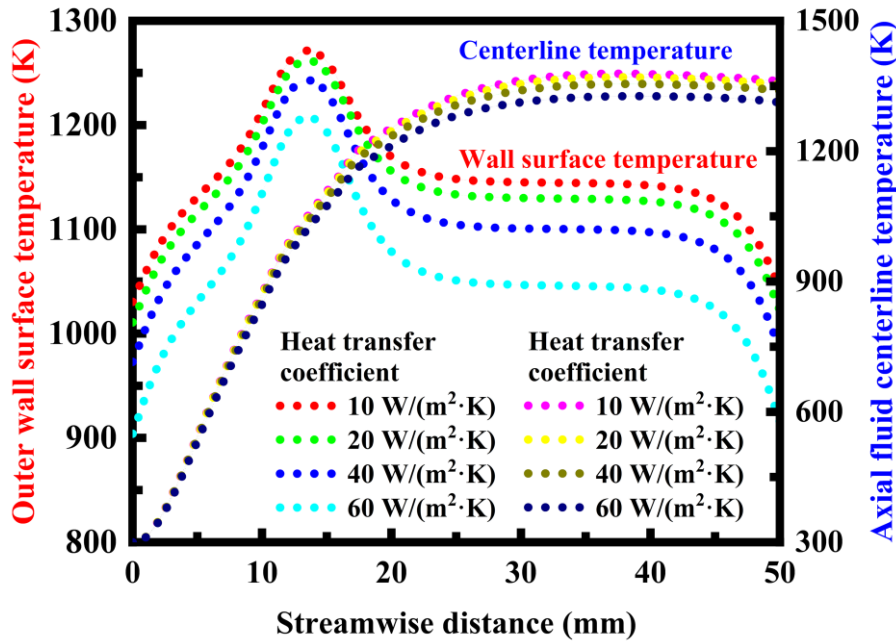


Figure 16. Temperature profiles along the outer wall surface of the burner and along the fluid centerline under different wall heat transfer coefficient conditions.

The variation characteristics of the combustion reaction rate along the fluid centerline are illustrated in Figure 17 under different wall heat transfer coefficient conditions. As the heat transfer coefficient increases, the reaction rate decreases due to increased heat losses, especially under very larger wall heat transfer coefficient conditions. However, the peak reaction rate remains unchanged, regardless of the wall heat transfer coefficient. Therefore, losses of combustion stability because of heat losses are a main issue that requires careful management of thermal energy for the burner. A means for thermal management should be provided. From a practical viewpoint, the walls of the cavity-stabilized burner should have a thermal conductivity that is anisotropic. The burner walls should inhibit transverse heat conduction but allow axial heat conduction. These burner walls with anisotropic heat conduction properties will allow upstream heat flux to preheat the incoming admixture of gases, yet not allow heat losses in the transverse direction. Alternatively, different suggestions have been made for facilitating the stability of flame in a micro-structured burner [55, 56]. To overcome the problem of heat losses involved in a micro-structured burner, catalytic

combustion has been demonstrated the advantages in terms of reduced heat losses [57, 58]. This approach can substantially eliminate the formation of oxides of nitrogen [59, 60] and greatly reduce heat loss, but surface transport is still a problem. Catalytically supported thermal combustion, which is a unique combination of catalytic and gas phase combustion, can achieve higher stability and obtain higher efficiency in operation than otherwise obtainable.

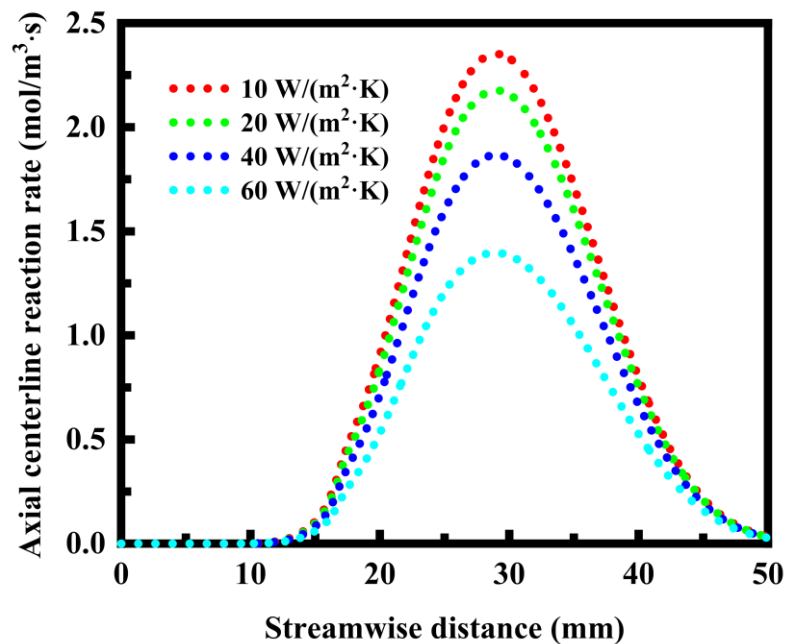


Figure 17. Axial centerline rate profiles of the combustion reaction under different wall heat transfer coefficient conditions.

3.6. Effect of fuel-air equivalent ratio

The temperature profiles along the outer wall surface of the cavity-stabilized burner and along the fluid centerline are presented in Figure 18 under different fuel-air equivalent ratio conditions. As the fuel-air equivalent ratio increases from 0.6 to 1.0, both the temperature along the fluid centerline and the temperature along the outer wall surface gradually increase. The amount of heat released by the combustion reaction increases due to the increased amount of the methane gas flowing into the cavity-stabilized burner. This is because when the fuel-air equivalent ratio is less than 1.0, the amount of the methane gas flowing into the cavity-stabilized burner per unit time is smaller than that in the case of complete combustion in which the equivalence ratio is 1.0. However, when the fuel-air equivalent ratio is increased from 1.0 to 1.2, both the temperature along the fluid centerline and the temperature along the outer wall surface decrease. This is because when the fuel-air equivalent ratio is greater than 1.0, the amount of the methane gas flowing into

the cavity-stabilized burner per unit time is greater than that in the case of complete combustion in which the equivalence ratio is 1.0. This will cause the relative content of oxygen gas required for complete combustion to decrease, resulting in insufficient combustion. In this case, incomplete combustion occurs, since there is not enough oxygen to allow methane to react completely in the cavity-stabilized burner. Therefore, when the equivalence ratio is 1.0, higher temperatures can be achieved in the cavity-stabilized burner, associated with higher combustion performance.

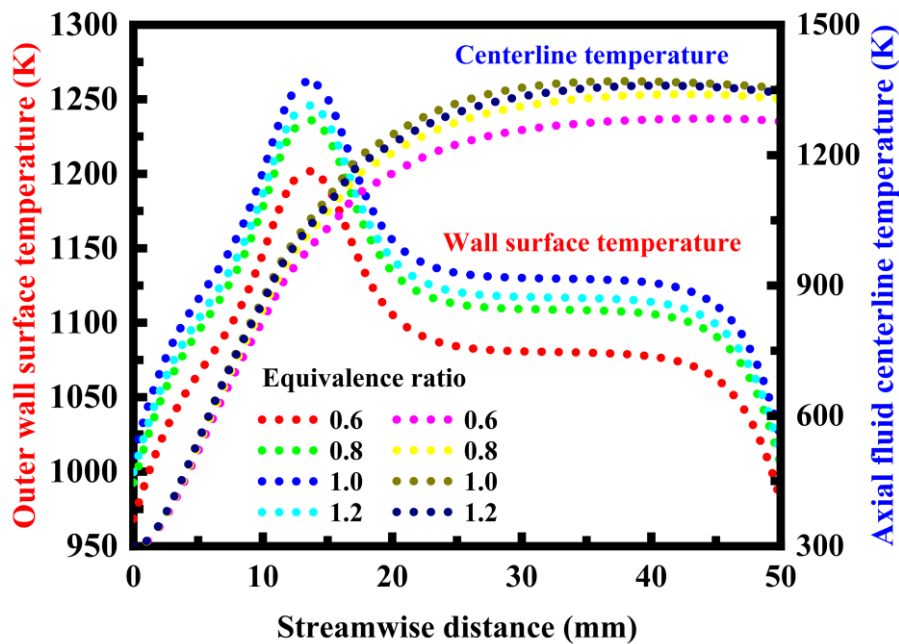


Figure 18. Temperature profiles along the outer wall surface of the burner and along the fluid centerline under different wall heat transfer coefficient conditions.

The effect of equivalence ratio on the fluid temperature at the outlet is investigated. The results are presented in Figure 19, in which the fluid temperature at the outlet is plotted against the equivalence ratio. The fluid temperature at the outlet indicates the enthalpy of flue gas. The equivalence ratio can be fuel-lean or fuel-rich. Combustion has been stabilized at an equivalence ratio as small as 0.4. With lean premixed combustion, the fuel-air equivalent ratio is smaller than 1.0. In this case, the fluid temperature at the outlet increases with the equivalent ratio of fuel to air, which increases power output of the cavity-stabilized burner. Use of an equivalent ratio of 1.0 permits complete combustion of the fuel, and therefore there is an optimum condition of maximal temperature. However, there is a dominant loss that is caused by sensible heat leaving with the flue gas. When the fuel-air equivalent ratio is greater than 1.0, the fluid temperature at the outlet decreases with the equivalent ratio of fuel to air, which is primarily caused by the amount of the

methane gas flowing into the cavity-stabilized burner, as discussed above. In this case, the amount of air flowing into the cavity-stabilized burner is smaller than the amount of air required for complete combustion. Therefore, only a portion of the total fuel is reacted in the cavity-stabilized burner. For the fuel-rich case, there are issues of efficiency loss, since the equivalent ratio should be limited to allow sufficient air for combustion in the cavity-stabilized burner.

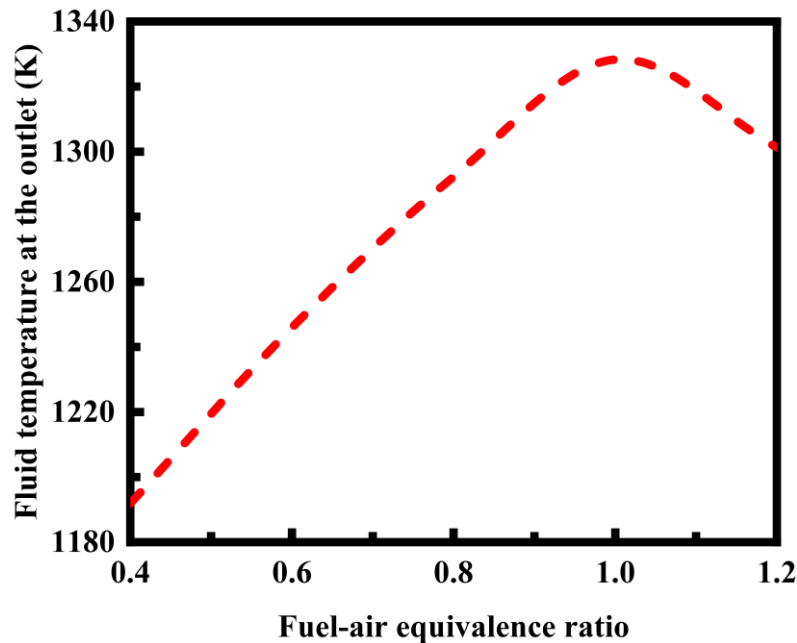


Figure 19. Axial centerline rate profiles of the combustion reaction under different wall heat transfer coefficient conditions.

4. CONCLUSIONS

Numerical simulations are conducted to gain insights into burner performance such as reaction rates, temperatures, species concentrations, and flames. The factors affecting combustion characteristics are determined for the cavity-stabilized burner. The major conclusions are summarized as follows:

- The inlet velocity of the mixture is a critical factor in assuring flame stability within the cavity-stabilized burner. There is a narrow range of inlet velocities that permit sustained combustion within the cavity-stabilized burner.
- Combustion is stabilized and flame stability is improved by recirculation of hot combustion products induced by the cavity structure.
- The thermal conductivity of the burner walls plays a vital role in flame stability. Burner walls

with low thermal conductivity will cause hot spots, and burner walls with high thermal conductivity are substantially isothermal.

- Improvements in flame stability are achievable by using walls with anisotropic thermal conductivity. Such walls with anisotropic heat conduction properties will allow upstream heat flux to preheat the incoming admixture of gases, yet not allow heat losses in the transverse direction.
- Burners with large dimensions lead to a delay in flame ignition and may cause blowout.
- Loss of flame stability due to external heat losses are main issues that require thermal management. Heat-insulating materials are favored to minimize external heat losses.
- There are issues of efficiency loss for fuel-rich combustion cases.

DECLARATION OF ETHICAL STANDARDS

The author of the paper submitted declares that nothing which is necessary for achieving the paper requires ethical committee and legal-special permissions.

CONTRIBUTION OF THE AUTHOR

Junjie Chen: Performed the computations, analyzed the results, and wrote the manuscript.

CONFLICT OF INTEREST

There is no conflict of interest in this study.

REFERENCES

- [1] Wegeng, R. S., Drost, M. K. "Developing new miniature energy systems", *Mechanical Engineering* 1994: 116(9); 82-85.
- [2] Ameel, T. A., Warrington, R. O., Wegeng, R. S., Drost, M.K. "Miniaturization technologies applied to energy systems", *Energy Conversion and Management* 1997: 38(10-13); 969-982.
- [3] Epstein, A. H. "Millimeter-scale, micro-electro-mechanical systems gas turbine engines", *Journal of Engineering for Gas Turbines and Power* 2004: 126(2); 205-226.
- [4] Epstein, A. H. "Millimeter-scale, MEMS gas turbine engines", *ASME Turbo Expo 2003, collocated with the 2003 International Joint Power Generation Conference*, June 16-19, 2003, Atlanta, Georgia, United States, Paper Number: GT2003-38866, Pages 669-696, Published Online: February 4, 2009, ISBN: 0-7918-3687-8, Conference Sponsors: International Gas

Turbine Institute.

- [5] Peterson, R. B. “Small packages. Miniaturization technologies applied to energy systems”, *Mechanical Engineering* 2001: 123(06); 58-61.
- [6] Kota, S., Ananthasuresh, G. K., Crary, S. B., Wise, K. D. “Design and fabrication of microelectromechanical systems”, *Journal of Mechanical Design* 1994: 116(4); 1081-1088.
- [7] Tadigadapa, S. A., Najafi, N. “Developments in microelectromechanical systems (MEMS): A manufacturing perspective”, *Journal of Manufacturing Science and Engineering* 2003: 125(4); 816-823.
- [8] Ananthasuresh, G. K., Howell, L. L. “Mechanical design of compliant microsystems-A perspective and prospects”, *Journal of Mechanical Design* 2005: 127(4); 736-7383.
- [9] E, J., Ding, J., Chen, J., Liao, G., Zhang, F., Luo, B. “Process in micro-combustion and energy conversion of micro power system: A review”, *Energy Conversion and Management* 2021: 246; 114664.
- [10]E, J., Luo, B., Han, D., Chen, J., Liao, G., Zhang, F., Ding, J. “A comprehensive review on performance improvement of micro energy mechanical system: Heat transfer, micro combustion and energy conversion”, *Energy* 2022: 239; 122509.
- [11]Wan, J., Fan, A. “Recent progress in flame stabilization technologies for combustion-based micro energy and power systems”, *Fuel* 2021: 286(2); 119391.
- [12]Gharehghani, A., Ghasemi, K., Siavashi, M., Mehranfar, S. “Applications of porous materials in combustion systems: A comprehensive and state-of-the-art review”, *Fuel* 2021: 304; 121411.
- [13]Ju, Y., Maruta, K. “Microscale combustion: Technology development and fundamental research”, *Progress in Energy and Combustion Science* 2011: 37(6); 669-715.
- [14]Chou, S. K., Yang, W. M., Chua, K. J., Li, J., Zhang, K. L. “Development of micro power generators - A review”, *Applied Energy* 2011: 88(1); 1-16.
- [15]Kim, J., Yu, J., Lee, S., Tahmasebi, A., Jeon, C. H., Lucas, J. “Advances in catalytic hydrogen combustion research: Catalysts, mechanism, kinetics, and reactor designs”, *International Journal of Hydrogen Energy* 2021: 46(80); 40073-40104.
- [16]Walther, D. C., Ahn, J. “Advances and challenges in the development of power-generation systems at small scales”, *Progress in Energy and Combustion Science* 2011: 37(5); 583-610.
- [17]Miwa, J., Asako, Y., Hong, C., Faghri, M. “Performance of gas-to-gas micro-heat exchangers”, *Journal of Heat Transfer* 2009: 131(5); 051801.
- [18]Marques, C., Kelly, K. W. “Fabrication and performance of a pin fin micro heat exchanger”,

- Journal of Heat Transfer* 2004: 126(3); 434-444.
- [19] Zhao, Z., Zuo, Z., Wang, W., Kuang, N., Xu, P. “Experimental studies on a high performance thermoelectric system based on micro opposed flow porous combustor”, *Energy Conversion and Management* 2022: 253; 115157.
- [20] Sadatakhavi, S. M. R., Tabejamaat, S., Zade, M. E. A., Kankashvar, B., Nozari, M. R. “Numerical and experimental study of the effects of fuel injection and equivalence ratio in a can micro-combustor at atmospheric condition”, *Energy* 2021: 225; 120166.
- [21] Guan, J., Lv, X., Spataru, C., Weng, Y. “Experimental and numerical study on self-sustaining performance of a 30-kW micro gas turbine generator system during startup process”, *Energy* 2021: 236; 121468.
- [22] Seo, J. M., Lim, H. S., Park, J. Y., Park, M. R., Choi, B. S. “Development and experimental investigation of a 500-W class ultra-micro gas turbine power generator”, *Energy* 2017: 124; 9-18.
- [23] Waitz, I. A., Gauba, G., Tzeng, Y. S. “Combustors for micro-gas turbine engines”, *Journal of Fluids Engineering* 1998: 120(1); 109-117.
- [24] Spadaccini, C. M., Mehra, A., Lee, J., Zhang, X., Lukachko, S., Waitz, I. A. “High power density silicon combustion systems for micro gas turbine engines”, *Journal of Engineering for Gas Turbines and Power* 2003: 125(3); 709-719.
- [25] Dessornes, O., Landais, S., Valle, R., Fourmaux, A., Burguburu, S., Zwysig, C., Kozanecki, Z. “Advances in the development of a microturbine engine”, *Journal of Engineering for Gas Turbines and Power* 2014: 136(7); 071201.
- [26] Nozari, M., Tabejamaat, S., Sadeghizade, H., Aghayari, M. “Experimental investigation of the effect of gaseous fuel injector geometry on the pollutant formation and thermal characteristics of a micro gas turbine combustor”, *Energy* 2021: 235; 121372.
- [27] Lee, D. H., Park, D. E., Yoon, E., Kwon, S. “A MEMS piston-cylinder device actuated by combustion”, *Journal of Heat Transfer* 2003: 125(3); 487-493.
- [28] Cunningham, C. S., Ransom, D., Wilkes, J., Bishop, J., White, B. “Mechanical design features of a small gas turbine for power generation in unmanned aerial vehicles”, *ASME Turbo Expo 2015: Turbine Technical Conference and Exposition*, June 15-19, 2015, Montreal, Quebec, Canada, Paper Number: GT2015-43491, V008T23A021, Published Online: August 12, 2015, ISBN: 978-0-7918-5679-6, Conference Sponsors: International Gas Turbine Institute.
- [29] Kaisare, N. S., Vlachos, D. G. “A review on microcombustion: Fundamentals, devices and applications”, *Progress in Energy and Combustion Science* 2012: 38(3); 321-359.

- [30] Maruta, K. "Micro and mesoscale combustion", *Proceedings of the Combustion Institute* 2011: 33(1); 125-150.
- [31] Dunn-Rankin, D., Leal, E. M., Walther, D. C. "Personal power systems", *Progress in Energy and Combustion Science* 2005: 31(5-6); 422-465.
- [32] Fernandez-Pello, A. C. "Micropower generation using combustion: Issues and approaches", *Proceedings of the Combustion Institute* 2002: 29(1); 883-899.
- [33] Lyons, K. M. "Toward an understanding of the stabilization mechanisms of lifted turbulent jet flames: Experiments", *Progress in Energy and Combustion Science* 2007: 33(2); 211-231.
- [34] Shanbhogue, S. J., Husain, S., Lieuwen, T. "Lean blowoff of bluff body stabilized flames: Scaling and dynamics", *Progress in Energy and Combustion Science* 2009: 35(1); 98-120.
- [35] Choi, J., Lee, W., Rajasegar, R., Lee, T., Yoo, J. "Effects of hydrogen enhancement on mesoscale burner array flame stability under acoustic perturbations", *International Journal of Hydrogen Energy* 2021: 46(74); 37098-37107.
- [36] McManus, K. R., Poinso, T., Candel, S. M. "A review of active control of combustion instabilities", *Progress in Energy and Combustion Science* 1993: 19(1); 1-29.
- [37] Sadanandan, R., Chakraborty, A., Arumugam, V. K., Chakravarthy, S. R. "Partially premixed flame stabilization in the presence of a combined swirl and bluff body influenced flowfield: An experimental investigation", *Journal of Engineering for Gas Turbines and Power* 2020: 142(7); 071010.
- [38] Kundu, K. M., Banerjee, D., Bhaduri, D. "On flame stabilization by bluff-bodies", *Journal of Engineering for Gas Turbines and Power* 1980: 102(1); 209-214.
- [39] Rasmussen, C. C., Driscoll, J. F., Hsu, K. Y., Donbar, J. M., Gruber, M. R., Carter, C. D. "Stability limits of cavity-stabilized flames in supersonic flow", *Proceedings of the Combustion Institute* 2005: 30(2); 2825-2833.
- [40] Kato, N., Im, S. K. "Flame dynamics under various backpressures in a model scramjet with and without a cavity flameholder", *Proceedings of the Combustion Institute* 2021: 38(3); 3861-3868.
- [41] Wang, S., Fan, A. "Combustion regimes of syngas flame in a micro flow reactor with controlled temperature profile: A numerical study", *Combustion and Flame* 2021: 230; 111457.
- [42] Ni, S., Zhao, D., You, Y., Huang, Y., Wang, B., Su, Y. "NO_x emission and energy conversion efficiency studies on ammonia-powered micro-combustor with ring-shaped ribs in fuel-rich combustion", *Journal of Cleaner Production* 2021: 320; 128901.

- [43] Westbrook, C. K., Dryer, F. L. “Simplified reaction mechanisms for the oxidation of hydrocarbon fuels in flames”, *Combustion Science and Technology* 1981: 27(1-2); 31-43.
- [44] Westbrook, C. K., Dryer, F. L. “Chemical kinetic modeling of hydrocarbon combustion”, *Progress in Energy and Combustion Science* 1984: 10(1); 1-57.
- [45] Jiménez, J. “Near-wall turbulence”, *Physics of Fluids* 2013: 25(10); 101302.
- [46] Celtek, M. S. “Turbulent flames investigation of methane and syngas fuels with the perspective of near-wall treatment models”, *International Journal of Hydrogen Energy* 2020: 45(60); 35223-35234.
- [47] Norton, D. G., Vlachos, D. G. “Combustion characteristics and flame stability at the microscale: a CFD study of premixed methane-air mixtures”, *Chemical Engineering Science* 2003: 58(21); 4871-4882.
- [48] Norton, D. G., Vlachos, D. G. “A CFD study of propane-air microflame stability”, *Combustion and Flame* 2004: 138(1-2); 97-107.
- [49] Leach, T. T., Cadou, C. P. “The role of structural heat exchange and heat loss in the design of efficient silicon micro-combustors”, *Proceedings of the Combustion Institute* 2005: 30(2); 2437-2444.
- [50] Leach, T. T., Cadou, C. P., Jackson, G. S. “Effect of structural conduction and heat loss on combustion in micro-channels”, *Combustion Theory and Modelling* 2006: 10(1); 85-103.
- [51] Chen, C. H., Ronney, P. D. “Scale and geometry effects on heat-recirculating combustors”, *Combustion Theory and Modelling* 2013: 17(5); 888-905.
- [52] Kaisare, N. S., Vlachos, D. G. “Optimal reactor dimensions for homogeneous combustion in small channels”, *Catalysis Today* 2007: 120(1); 96-106.
- [53] Xu, X., Pereira, L. F. C., Wang, Y., Wu, J., Zhang, K., Zhao, X., Bae, S., Bui, C. T., Xie, R., Thong, J. T. L., Hong, B. H., Loh, K. P., Donadio, D., Li, B., Özyilmaz, B. “Length-dependent thermal conductivity in suspended single-layer graphene”, *Nature Communications* 2014: 5; 3689.
- [54] Wei, Z., Ni, Z., Bi, K., Chen, M., Chen, Y. “In-plane lattice thermal conductivities of multilayer graphene films”, *Carbon* 2011: 49(8); 2653-2658.
- [55] Liu, W., Wang, L., Su, S., Wu, Z., Guo, Y., Du, K. “Study of the flame flow and combustion characteristics of pool fires around a bluff body in the ship engine room”, *Case Studies in Thermal Engineering* 2021: 28; 101514.
- [56] Huang, Y., He, X., Jin, Y., Zhu, H., Zhu, Z. “Effect of non-uniform inlet profile on the combustion performance of an afterburner with bluff body”, *Energy* 2021: 216; 119142.

- [57] Yan, Y., Wu, G., Huang, W., Zhang, L., Li, L., Yang, Z. “Numerical comparison study of methane catalytic combustion characteristic between newly proposed opposed counter-flow micro-combustor and the conventional ones”, *Energy* 2019: 170; 403-410.
- [58] Rodrigues, J. M., Ribeiro, M. F., Fernandes, E. C. “Catalytic activity of electrodeposited cobalt oxide films for methane combustion in a micro-channel reactor”, *Fuel* 2018: 232; 51-59.
- [59] Miller, J. A., Bowman, C. T. “Mechanism and modeling of nitrogen chemistry in combustion”, *Progress in Energy and Combustion Science* 1989: 15(4); 287-338.
- [60] Glarborg, P., Miller, J. A., Ruscic, B., Klippenstein, S. J. “Modeling nitrogen chemistry in combustion”, *Progress in Energy and Combustion Science* 2018: 67; 31-68.